Development of a colorimetric microfluidic pH sensor for autonomous seawater measurements

Victoire M.C. Rérolle [a],[*], Cedric F.A. Floquet [b], Andy J.K. Harris [b], Matt C. Mowlem [b], Richard R.G.J. Bellerby [c],[d],[e], Eric P. Achterberg [a]

[a] University of Southampton, National Oceanography Centre, Southampton, Southampton SO14 3ZH, UK
[b] National Oceanography Centre, Southampton SO14 3ZH, UK
[c] Norwegian Institute for Water Research, Thormøhlensgate 53D, Bergen N-5006, Norway
[d] Uni Bjerknes Centre, Uni Research AS, Allégaten 55, Bergen N-5007, Norway
[e] Geophysical Institute, University of Bergen, Allégaten 70, Bergen N-5007, Norway

HIGHLIGHTS

- Automated bench-top spectro-photometric pH sensor for shipboard deployment.
- Microfluidic design to miniaturize the colorimetric pH sensor and reduce reagent consumption.
- Robust optical set up using LEDs.
- Accurate and precise pH sensor.
- pH measurements in seawater at *in situ* temperature.

GRAPHICAL ABSTRACT
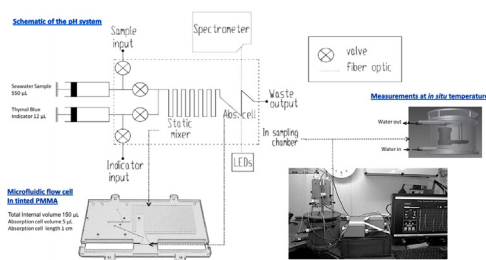
ARTICLE INFO

ABSTRACT

High quality carbonate chemistry measurements are required in order to fully understand the dynamics of the oceanic carbonate system. Seawater pH data with good spatial and temporal coverage are particularly critical to apprehend ocean acidification phenomena and their consequences. There is a growing need for autonomous *in situ* instruments that measure pH on remote platforms. Our aim is to develop an accurate and precise autonomous *in situ* pH sensor for long term deployment on remote platforms. The widely used spectrophotometric pH technique is capable of the required high-quality measurements. We report a key step towards the miniaturization of a colorimetric pH sensor with the successful implementation of a simple microfluidic design with low reagent consumption. The system is particularly adapted to shipboard deployment: high quality data was obtained over a period of more than a month during a shipboard deployment in northwest European shelf waters, and less than 30 mL of indicator was consumed. The system featured a short term precision of 0.001 pH ($n = 20$) and an accuracy within the range of a certified Tris buffer (0.004 pH). The quality of the pH system measurements have been checked using various approaches: measurements of certified Tris buffer, measurement of certified seawater for DIC and TA, comparison of measured pH against calculated pH from pCO_2, DIC and TA during the cruise in northwest European shelf waters. All showed that our measurements were of high quality. The measurements were made close to *in situ* temperature (+0.2 °C) in a sampling chamber which had a continuous flow of the ship's underway seawater supply. The optical set up was robust and relatively small due to the use of an USB mini-spectrometer, a custom made polymeric flow cell and an LED light source. The use of a three wavelength LED with detection that integrated power across the whole of each LED output spectrum indicated that low wavelength resolution detectors can be used instead of the current USB mini

* Corresponding author. Tel.: +44 023 80596168; fax: +44 023 80593059.
E-mail addresses: Victoire.Rerolle@noc.ac.uk, Victoire.Rerolle@noc.soton.ac.uk (V.M.C. Rérolle).

spectrophotometer. Artefacts due to the polychromatic light source and inhomogeneity in the absorption cell are shown to have a negligible impact on the data quality. The next step in the miniaturization of the sensor will be the incorporation of a photodiode as detector to replace the spectrophotometer.

1. Introduction

Miniaturization of analytical systems has led to a reduction in sample, reagent and power consumption. A key advance in wet chemical sensors has been the implementation of microfluidic Lab-on-Chip platforms. Microfluidic technology has a range of applications in clinical, biological and chemical analyses of small volume samples [1]. The technology is of great interest for environmental monitoring, in particularly in aquatic systems [2].

Oceans play an important role in climate regulation [3]. The oceans have taken up *ca.* 25% of anthropogenic CO_2, resulting in changes to the carbonate system [4]. This process is termed ocean acidification and impacts on marine ecosystems [5] and the ocean's capacity to absorb future atmospheric CO_2 emissions [6]. Average surface ocean pH has decreased by 0.1 pH units since the onset of the industrial revolution [7], and currently a decrease of 0.002 pH units per year is observed [8–10]. Monitoring such changes requires sensors with high precision and accuracy. Despite important efforts to develop new instruments and coordinate international monitoring activities of the ocean's carbonate system [11], routine high resolution oceanic measurements using moorings, drifters, or profiling floats are currently limited to temperature, salinity, oxygen and recently nutrients [12]. High resolution carbonate chemistry measurements (*e.g.* pH, pCO_2, total alkalinity (TA)) are urgently required in order to observe the ocean acidification phenomena and study its consequences. Large scale monitoring of carbonate chemistry in the oceans will only be possible with low cost sensors featuring low power and reagent consumption. The widely used spectrophotometric pH technique is capable of the high-quality measurements required to study the changes in the marine carbonate system [13]. High precision and accuracy pH measurements using the spectrophotometric technique have been demonstrated at sea for surface water measurements on research vessels [14–21], and more recently, successful *in situ* deployments have been reported [22–26]. This simple and high precision technique is a prime candidate for miniaturization and would address the urgent need for ruggedized autonomous *in situ* pH instruments. Furthermore the spectrophotometric method is calibration free, which is ideal for long-term deployments on remote platforms.

Here we report a low cost spectrophotometric pH sensor with high precision and accuracy. The system uses a simple micro-fluidic design integrated in a shipboard instrument with low reagent consumption. A robust optical set up is achieved with the use of a custom-made polymeric flow cell coupled to a three wavelength Light Emitting Diode (LED). This work forms a key step towards the development of a fully integrated microfluidic pH analyser for *in situ* deployment.

2. Principle of the spectrometric method

The spectrophotometric pH determination is based on the addition to a seawater sample of a pH indicator dye with coloured protonated and deprotonated species. The acid and base forms of the indicator have different absorption spectra. The colour of the solution (sample with indicator) is pH dependent as it varies with the relative amount of the two indicator species. The pH of a sample is determined from the acid dissociation constant ($pK_{ind} =$ $-\log_{10}(K_{HI^-})$) and the absorbance ratio of the deprotonated (I^{2-}) and protonated (HI^-) indicator forms using equation 1 [27]:

$$pH = pK_{ind} + \log_{10}\left(\frac{R - e_1}{e_2 - Re_3}\right) \qquad (1)$$

with $R = A_1/A_2$, $e_1 = \varepsilon_1(HI^-)/\varepsilon_2(HI^-)$, $e_2 = \varepsilon_1(I^{2-})/\varepsilon_2(HI^-)$ and $e_3 = \varepsilon_2(I^{2-})/\varepsilon_2(HI^-)$). A_1 and A_2 refer to the absorbances at wavelengths 1 and 2. $\varepsilon_\lambda(I^{2-})$ and $\varepsilon_\lambda(HI^-)$ are the molar absorptivity coefficients at wavelength λ (with subscripts 1 and 2 corresponding to the wavelengths at maximum absorptivity of the basic and acidic forms of the indicator respectively) of the base (I^{2-}) and acid (HI^-) forms of the dye, respectively.

The molar absorptivity coefficients and the pK_{ind} are functions of temperature and salinity.

The pH measurements are inherently calibrated as only the absorbance ratio (R) of the two indicator forms is required to calculate the pH of a sample, and not the exact total concentration of the indicator. The pH indicator solution characteristics (ε_1, ε_2, pK_{ind}), as a function of temperature and ionic strength (I), need to be determined in the laboratory prior to instrument deployment.

3. Materials and methods

3.1. Chemical preparation

3.1.1. Indicator solution

A 2 mM thymol blue indicator solution was prepared by dissolution of thymol blue sodium salt (ACS Reagent, $C_{27}H_{29}NaO_5S$, Sigma–Aldrich 861367) in deionised water (MilliQ, Millipore, >18.2 mΩ cm^{-1}). The solution was left to equilibrate overnight and the pH was adjusted to *ca.* 8.1 using a 1 M sodium hydroxide solution (NaOH, Fisher Scientific S/4920/53). The pH of the solution was verified with a glass electrode (LL Combined Unitrode PT 1000 WC-Electrode, Metrohm UK Ltd). The indicator solution was stored in a gas tight nutrition bag (Flexboy® Bags, Sartorius Stedim Biotech) wrapped in aluminium foil to avoid photo-bleaching.

3.1.2. Acid buffers and basic solutions

Acidic buffer solutions of pH $\approx$ 5 were prepared using acetic acid ($C_2H_4O_2$, Fisher Scientific A/0400/PB08), sodium acetate trihydrate ($C_2H_3NaO_2 \cdot 3H_2O$, Fisher Scientific S/2000/53) and sodium chloride (NaCl, Fisher Scientific S/3160/53) [18,28]. Basic solutions of pH $\approx$ 10 were prepared by dissolution of NaCl in deionized water and adjustment of the pH with 1 M NaOH [18,28]. Both acidic and basic solutions were prepared at four salinities: 22.5, 27.5, 32.5 and 37.5 PPT. The pH of the solutions was verified with a glass pH electrode.

3.2. Instrument

3.2.1. System overview and principles of operation

A schematic representation of the pH system is presented in Fig. 1A. Syringe pumps (Nanomite, Harvard Apparatus, UK) were used to propel the seawater sample (550 μL) and the thymol blue indicator (12 μL). Four micro-inert valves (LFNA1250125H, Lee Products Ltd., UK) controlled the fluid distribution. The reagent and sample streams were mixed in the flow cell in a static mixer before entry into the absorption cell. The light source was formed by a three wavelength LED (435 nm (25 nm full width half
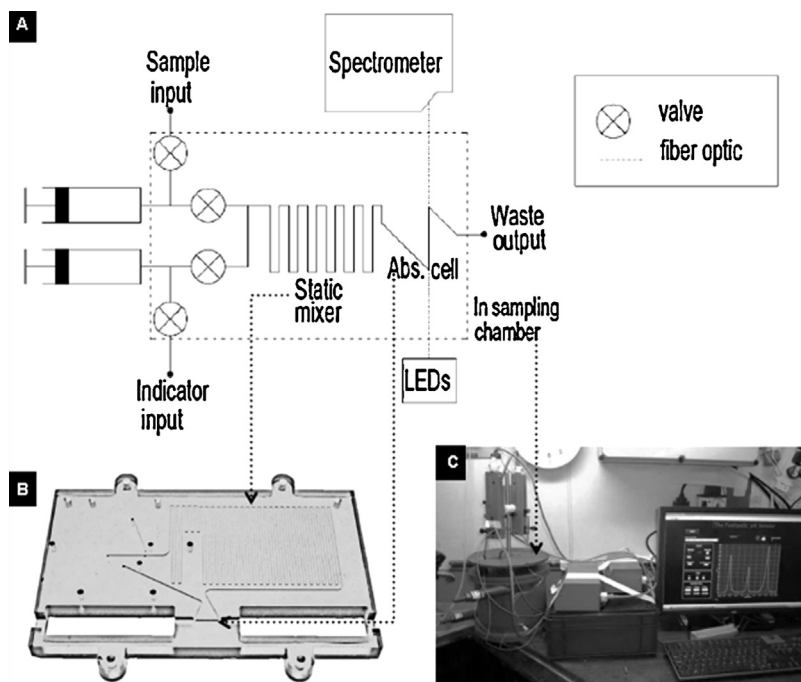
Fig. 1. Details of the pH system. (A) Schematic representation of the pH system. The seawater sample and indicator solution are pumped by two different syringe pumps and mixed in the flow cell in a static mixer before entering the absorption cell. The LEDs' light transmitted through the absorption cell is recorded by the HR4000 spectrometer. The measurement is made close to *in situ* temperature (+0.2 °C) by placement of the microfluidic flow cell in the sampling chamber which has a continuous flow of the ship's underway seawater supply. (B) Microfluidic flow cell milled in tinted PMMA. All the cross sections of the channels are 250 μm × 250 μm except for the absorption cell which is 700 μm × 700 μm. (C) Picture of the pH set up aboard the RRS discovery. The sampling chamber is on the left with the two syringe pumps on top. The electronic control box, light source and detector are in the middle and the computer is on the right.

maximum (FWHM)), 596 nm (15 nm FWHM), and 750 nm (30 nm FWHM), Roithner Laser, Austria), and light transmitted through the absorption cell was recorded by a spectrometer (grating: 300 Line Composite Blaze and Slit width: 5 μm, HR4000, Ocean Optics Inc., UK). The system was controlled by computer with custom software (written in LabView 9) using a control card (PCI 6289, National Instruments Inc., UK). Custom electronics boards were developed to interface the valves, light sources and thermistors. The measurements were made at temperatures close (+0.2 °C) to the *in situ* surface ocean values. During the measurement cycle, the flow cell was first rinsed with 300 μL of sample before injection of 12 μL of indicator and the determination of the absorption spectra. The remainder of the sample was pumped through the system at a rate of 60 μL min⁻¹. Measurements of pH at multiple indicator concentrations at the end tail of the dilution/dispersion curve of the indicator aliquot in the sample stream after passing through a static mixer were used to quantify the perturbation of the sample pH by the indicator by linear regression [24,26]. A complete analysis cycle of a seawater sample took 6 min.

3.2.2. Microfluidic flow cell and mixer

The microfluidic flow cell comprised the absorption cell and static mixer and was manufactured in tinted poly(methyl methacrylate) (PMMA) (Fig. 1B). The fabrication method of the cell is described in detail in Ogilvie et al. and Floquet et al. [29,30], and has been successfully applied for nutrient micro-analysers [30–32]. All channel cross sections were 250 μm × 250 μm, except for the absorption cell which was 700 μm × 700 μm. The static mixer was a long (2.2 m) serpentine shaped channel.

3.2.3. Optical set up

The light source used in our pH system was a tri-coloured LED with wavelengths of 435 nm (25 nm FWHM) and 596 nm (15 nm FWHM) corresponding to the absorption maxima of the indicator

forms (HI⁻ and I²⁻), and 750 nm (30 nm FWHM) to monitor the sample turbidity and Schlieren effect (Fig. 2). The three individual single wavelength LED dies were mounted in a single package (TO-98) to create the tri-coloured LED.

A linear array photodiode spectrometer (HR4000, Ocean Optics, UK) was used as detector. To improve the signal to noise ratio, absorbances at the three wavelengths were measured by integration of the light signal on the full spectrum of the LED. The light source and detector were connected to the microfluidic chip by two optical fibres (600 μm diameter, Thorlabs, USA).
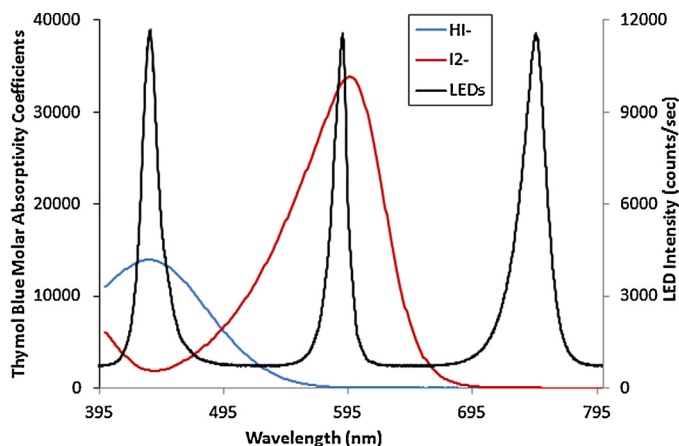

Fig. 2. Thymol blue indicator and light source spectra. Molar absorptivity coefficient spectra of the basic (I²⁻ in red) and acidic (HI⁻ in blue) forms of the thymol blue indicator. The light spectrum of the tri-coloured LED is shown in black. (For interpretation of the references to color in this figure legend, the reader is referred to the web version of the article.)

3.2.4. Measurement at in situ temperature

The pH measurements were undertaken at *in situ* surface temperature by submersion of the microfluidic chip in the sampling chamber which was continuously flushed using surface seawater (Fig. 1C).

To avoid channel blockage and light scattering by particulates, an *in line* filter (0.45 μm pore size, Millex HP syringe filter Millipore Express® (PES) membrane 33 mm diameter, Millipore) was placed at the entry of the sample tube.

3.3. Indicator solution characterization: determination of the extinction coefficients

The pK_2 for the thymol blue indicator as determined by Zhang and Byrne [33] was used ($K_2 = [H^+]_T[I^{2-}]/[HI^-]$ where $[H^+]_T$ is the total hydrogen ion concentration in seawater (mol kg^{-1})) [33].The molar absorption coefficients of the batch of thymol blue indicator were determined for the temperature and salinity ranges encountered during our deployments in tropical and temperate surface ocean waters (T = 8–26 °C and S = 22.5–37.5 PPT).The molar extinction coefficients of the acid indicator form (HI$^-$) at wavelengths 435 nm and 596 nm were determined in the acidic buffer. The basic solution was used to obtain the coefficients of the basic form (I^{2-}) of the dye. The absorbance contributions of both forms of indicator (I^{2-} and HI$^-$) were taken into account in the determination of the molar absorptivity coefficient [18,33]. Absorbances at the three wavelengths were measured by integration of the light signal on the full spectrum of the LED. Absorbance of the indicator in each buffer solution was measured at five concentrations. A 1 cm absorption cell was used to determine $\varepsilon_{435}(HI^-)$ and $\varepsilon_{596}(I^{2-})$, and a 10 cm cell was used to determine $\varepsilon_{596}(HI^-)$ and $\varepsilon_{435}(I^{2-})$. The cells were made in PMMA using the design and fabrication method outlined above. Measurements of the 5 indicator concentrations for each of the four salinities (22.5, 27.5, 32.5 and 37.5 PPT) were performed at 5 temperatures (8, 12, 17, 22 and 26 °C). The temperature and salinity dependencies of the extinction coefficients were estimated *via* stepwise multiple linear regressions of the experimental results with T, T^2, S and S^2. A *t*-test was performed to check which variable was important to the model of the e_i coefficients as a function of temperature and salinity and an *F*-test was used to determine if the model was adequate.

3.4. Cruise deployment

The pH sensor has been deployed on cruise D366 as part of the UK Ocean Acidification Research Program. The automated pH system was operated continuously on the underway seawater supply in the period between 06/06/2011 and the 07/07/2011. Only 5 μL of indicator was injected per sample during the deployment instead of 12 μL in the later configuration. The volume of indicator was increased after the deployment in order to reduce the Schlieren effect observed during the deployment (see Section 4.6). Three bottles of certified Tris buffer (batch 7) provided by the Scripps Institution of Oceanography have been analyzed at the beginning, the middle and the end of the cruise in order to evaluate the stability of the system. All pH values in this study are reported using the total pH scale (pH$_{tot}$), as this is the most commonly used pH scale, and importantly the only available certified pH buffer (Tris from Scripps) has been certified on this pH scale.

4. Results and discussion

4.1. Indicator characterization

Accounting for the presence of the two indicator species in the acidic and basic solutions resulted in a correction of up to 11% on e_1, 1% on e_2 and 5% on e_3. The coefficients of the multiple variables regressions as well as the statistical analysis results are detailed in Table 1.

The discrepancy between pH values calculated with these coefficients and values calculated with coefficients from Zhang and Byrne [33] was about 0.02, and varied between 0.015 and 0.029 pH units. Apparent extinction coefficients are influenced by the wavelength resolution of the detector. Zhang and Byrne used the Varian Instruments Cary 17D and Cary 3 spectrophotometers with a wavelength resolution of *ca.* 1–2 nm. We estimated that about 0.015 pH units of the observed discrepancy was due to the wide wavelength resolution in our system resulting from integration on the whole LED peak (LED's FWHM = 15–20 nm). Impurities in the indicators also affected the coefficients [34,35] but to a smaller extent (about 0.005 pH units). The latter was estimated by comparing our pH values with those calculated with a wavelength resolution as narrow as 0.3 nm and coefficients from Zhang and Byrne. The consistency and the magnitude of this discrepancy demonstrated that it was correct to integrate the signal under the whole LED peak. The magnitude of the discrepancy due to the wide wavelength resolution highlighted the importance of the indicator characterization when using a system with wider wavelength resolution than the systems used to obtain the indicators' extinction coefficients and reported in the literature [13]. Finally, the variability in the observed discrepancy was mainly due to the fact that the salinity dependence of the extinction coefficient ε_{596}^{12-} was taken into account in our model whereas it was not in the model from Zhang and Byrne.

4.2. Implementation of the PMMA microfluidic flowcell

The tinted PMMA reduces the stray light that reaches the detector resulting in a general enhancement of the systems' sensitivity and of the signal to noise ratios [30]. The use of a static mixer instead of active mixing systems reduces power consumption and is more straightforward to incorporate in the custom designed PMMA flow cell. Benchtop pH systems typically use 100 mm pathlength cuvettes [16,18,20,36,37] with enhanced sample to indicator mixing ratios (700:1 to 1000:1) in order to minimize the impact of the indicator addition on the sample pH [38]. Similar to work by Martz et al. [24] and Seidel et al. [26] in macro fluidic systems we addressed the impact of the indicator on sample pH by measurement of the pH over a wide range of mixing ratios (1:25 to 1:80) and using this data to regress back to a theoretical pH when no indicator was present (see Fig. 3 in Section 4.3). This range in mixing ratios was created by providing a short (7 s, 12 μL) pulse of indicator into the flow cell. This pulse is dispersed in the long serpentine mixer by "Taylor Aris" dispersion resulting from the fluid flow reduction near the channel walls due to enhanced friction [39,40]. The dispersion produces a near Gaussian indicator concentration profile in the sample stream in time and space. A sample flow rate of 60 μL min^{-1} was used in order to obtain an enhanced dispersion and a homogenous mixing across the channel. A 10 mm long absorbance cell was used in our design in order to minimize deviations from the Beer Lambert's law (see Section 4.4.2). This approach allowed us to use flow rates which were sufficiently high to maintain a good control of the pumps. The simple design of this microfluidic platform proved to be very efficient as it enabled effective mixing of the indicator with the sample, and allowed pH measurements and correction of the indicator effect on the sample pH with a single addition of indicator.

4.3. Correction for indicator induced pH perturbation

The interpolation of pH to a zero indicator concentration was undertaken using a weighted linear regression (see Fig. 3B),

Table 1
Coefficients derived from multiple linear regression analysis, with results of statistical analysis.

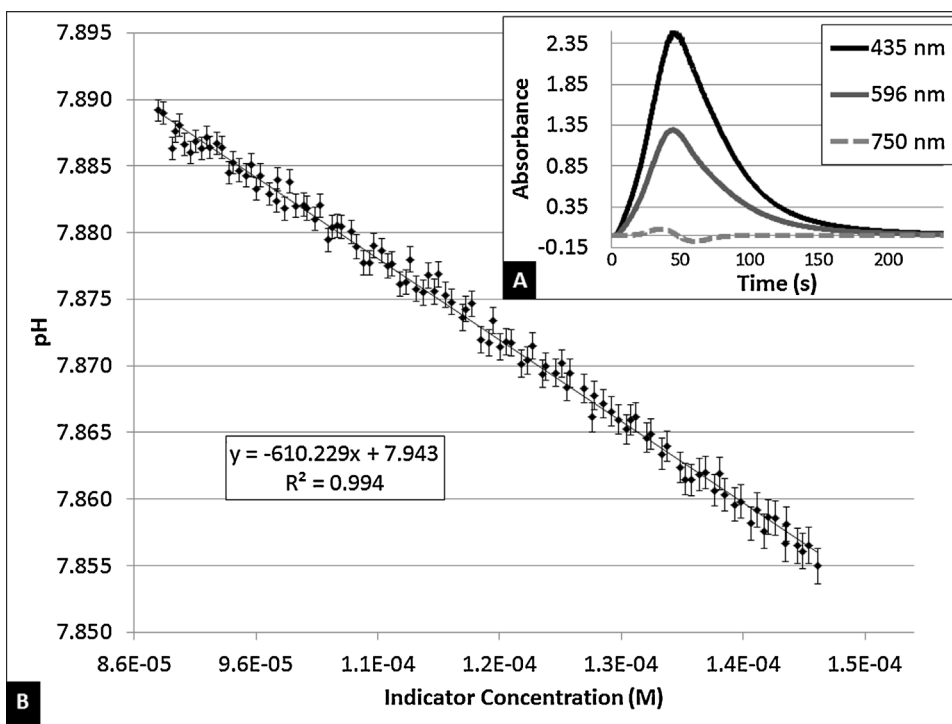| Parameter	Intercept	T	T^2	S	S^2	F-test	Prob > F	R^2	MSE
ε^{HI-}_{435}	13,506		−0.535			21.22	2.52E−4	0.555	1.18E4
ε^{HI-}_{596}	99.221	−3.321	0.126			71.25	5.44E−9	0.893	8.13
$\varepsilon^{I^{2-}}_{435}$	2271.2		0.147			5.30	0.03	0.238	3.86E3
$\varepsilon^{I^{2-}}_{596}$	41,881	51.015		755.033	13.453	7.71	0.002	0.591	2.50E5

MSE: mean square error; Prob: probability.

Fig. 3. Correction for indicator induced pH perturbation. (A) Absorbances at wavelengths 435, 596 and 750 nm as a function of time (s) as the indicator plug passes through the flow cell. (B) pH as a function of indicator concentration (M). The end tail of the absorbance plug was used to calculate pH as a function of indicator concentration and is interpolated to a zero indicator concentration. The corrected pH is 7.943 in this example.

whereby the weights were the inverse of the squared error (noted u) on pH at each concentration $(1/u_{pH}([ind])^2)$. The error on pH (Eq. (4)) was calculated as the square root of the sum of the squares of the estimated uncertainties of the method (*e.g.* the indicator pK and molar absorptivities, the accuracy of the temperature, salinity and absorption measurements).

$$u_{pH} = \sqrt{\left(\frac{\partial pH}{\partial pK_2} \cdot u_{pK_2}\right)^2 + \left(\frac{\partial pH}{\partial R} \cdot u_R\right)^2 + \left(\frac{\partial pH}{\partial e_1} \cdot u_{e_1}\right)^2 + \left(\frac{\partial pH}{\partial e_2} \cdot u_{e_2}\right)^2 + \left(\frac{\partial pH}{\partial e_3} \cdot u_{e_3}\right)^2} \qquad (4)$$

The best linear fits to correct for the indicator addition were obtained with absorbance values ranging from 0.55 and 1.65 (RMS > 0.99]). The mean magnitude of the correction was 0.02 ± 0.01 pH units during the cruise deployment of the analytical system. The estimated standard error of the corrected pH was on average 0.0005 ± 0.0003 pH units.

4.4. Deviations from Beer's law of absorbance behaviour

4.4.1. Deviation due to the polychromatic light source

The sensitivity of the absorbance measurement to signal variations and linearity of the Beer's law are affected by signal poly-chromaticity in the case that a non-monochromatic light source is used [41]. The bandwidth ratio of the absorbance profile to the light source spectra was between 3 and 5 in our system. It was therefore important to verify that the sensitivity of the absorbance measurements was not affected by the integration of the signal over the full LED peak [41]. Integration over the full LED peak resulted indeed in a small negative deviation of the apparent absorbance compared to the peak absorbance obtained with the single maximum absorption wavelength (Fig. 4A and B). These effects were due to the fact that absorptivities are not constant across the spectral emission bands of the LEDs. The sensitivity of the detector also varies with the wavelength resulting in a skewing of the LED emission spectra towards the high wavelength side of the bands [42]. In addition, the peak of the emission bands may not be well centred on the absorption peak of the indicator species. The linearity of the curves was verified with the range of the relative sensitivity ($S = A_{apparent}/A_{peak}$) as a function of the peak absorbance [41] (Fig. 4C). Although there was a deviation from Beer's law ($S \approx 0.97$ instead of 1), the absorbance range is still in the linear range of Beer's law (within the $\pm 5\%$ tolerance range). Integration of the signal on the full LED spectrum was therefore considered to be appropriate to calculate the absorbance values.
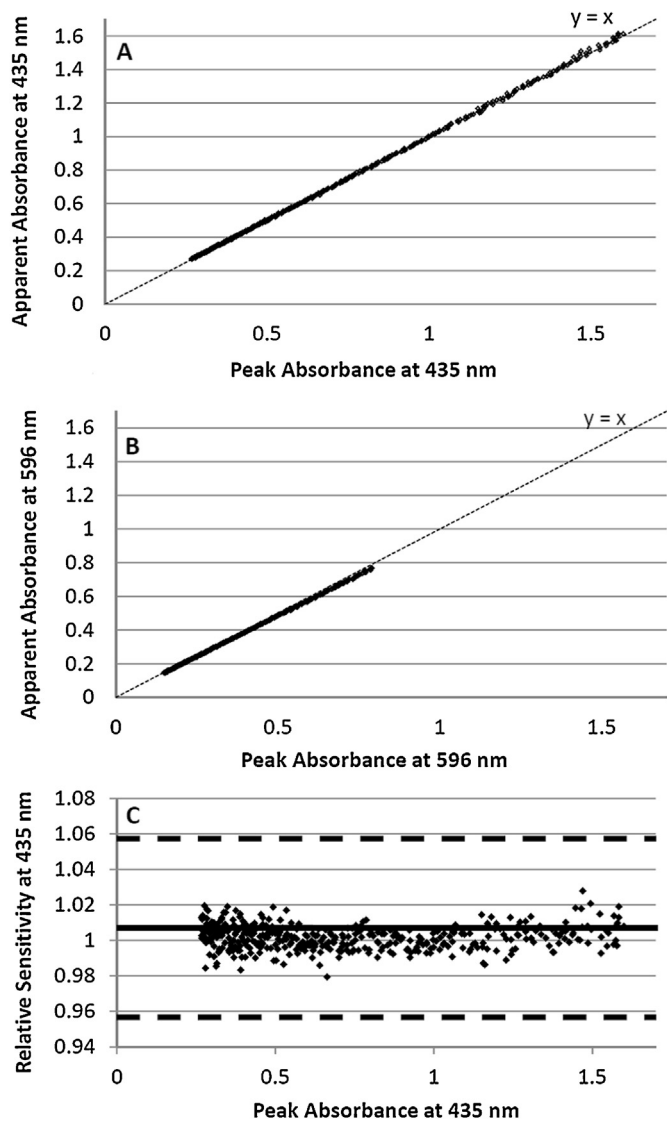
Fig. 4. Sensitivity analysis. (A and B) Apparent absorbance (using the whole LED peak) *versus* peak absorbance (using a single pixel). The dotted line represents the case when the peak absorbance equals the apparent absorbance. (C) Linearity plot for the LED centred on 435 nm. The line represents the linear case and the dotted line represents the −5% tolerance interval.

Table 2
Precision and accuracy of certified Tris buffer measurements.

Average discrepancy between certified pH and measured value for Tris buffer ($n = 20$)	Precision (pH unit) of replicate Tris buffer analyses ($n = 20$)	Date of analysis
0.0007	0.0007	11/06/2011
0.0021	0.0009	23/06/2011
0.0025	0.0011	07/07/2011

Beer Lambert's law due to indicator gradients was therefore also deemed negligible in our system.

4.5. Advantages of the measurements at in situ temperature

The insertion of the microfluidic chip in the sampling chamber simplified the set-up, minimized potential CO_2 exchange with the atmosphere and resulted in a minor temperature discrepancy between the sampling chamber (*i.e.* measurement temperature) and *in situ* seawater temperatures in the ocean. This approach therefore minimized the requirement for temperature correction of pH data as is the case for thermostatted (*e.g.* 25 °C) measurements. During the pH system deployment on a cruise in European shelf seas in 2011, we observed a temperature difference between the surface ocean and the measurement chamber of only 0.2 ± 0.06 °C.

4.6. System precision and accuracy

The performance of the system has been evaluated through pH analysis at 25 °C of three bottles of certified Tris buffer (batch 7). The temperature was controlled to 0.01 °C by placement of the flow cell in a temperature controlled water bath (Techne-10A Tempette). During the five weeks of deployment of the instrument at sea, we obtained a short term precision of 0.0009 pH unit ($n = 20$) and pH values within the reported range of the certified Tris buffer (0.004 pH units) (Table 2).

In order to estimate the precision of the system for natural seawater analyses at sea during the cruise, the standard deviation of 20 consecutives measurements was determined at three different locations. The locations were chosen where the ship was maintained in position sufficiently long to obtain 20 measurements in similar water masses. Although this is not ideal as the water mass characteristics vary with time, it gives a first estimate of system precision for replicated natural seawater analysis. The precision at the three locations was found to vary between 0.0008 and 0.0017 pH units ($n = 20$).

Measurement accuracy is affected by the accuracy of the indicator extinction coefficients and pK_2, the indicator perturbation correction method, and the accuracy of the temperature and salinity measurements. The analysis of the Tris buffer demonstrated the good accuracy of our indicator characterization (within 0.004 pH units) at 25 °C and salinity 35. However, the Tris buffer analyses are less strongly affected by pH perturbations from the indicator additions than seawater and are therefore not appropriate to verify the indicator pH correction method. Comparison of cruise pH data with pH calculated from a pair of the carbonate parameters DIC, TA and pCO_2 showed a discrepancy between 0.005 and 0.013 pH units. Calculations were made using CO2SYS [44], on the total pH scale with K_1 and K_2 from Mehrbach et al. [45], refitted by Dickson and Millero [46] and KHSO_4 from Dickson [47].

Part of the pH offset was likely due to the Schlieren effect impacting the indicator perturbation correction method because of the low ionic strength ($I = 2$ mM) of the indicator solution compared to the sample. The Schlieren effect was evidenced here by absorption variations at 750 nm (Fig. 3A). This phenomenon was noticeable at strong concentration gradients and resulted in non-linearity of the
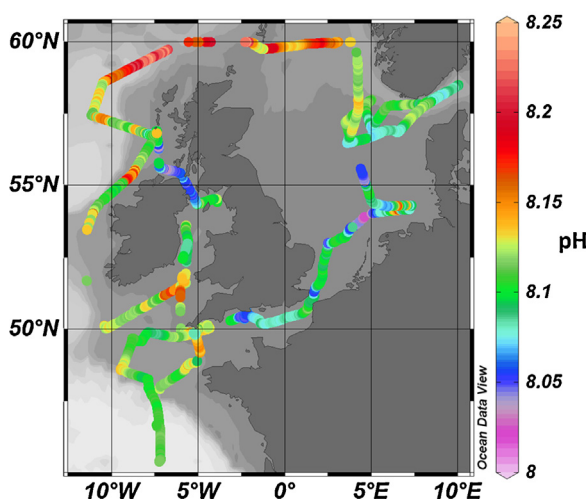
4.4.2. Deviation due to indicator gradient in the absorption cell

The indicator gradient along the absorption cell length will lead to a systematic pH measurement error due to a deviation from the Beer Lambert's law condition. The error depends on the dispersion length of the indicator plug and the length of the optical cell. The dispersion length of the indicator after its passage through the static mixer in our microfluidic flowcell was estimated using a model based on Taylor–Aris dispersion theory [39,43]. The concentration distribution obtained with the model, with an 8 μm resolution, was used to calculate pH assuming a linear relationship between the indicator concentration and pH. Absorbances at the two wavelengths of interest were deduced from pH and indicator concentration at every data point and then summed in order to obtain the absorbances of a 1 cm optical path length. These absorbances were processed using the same procedure as for sample measurements. The pH estimated from the linear regression was 0.0001 pH units lower than the actual pH of the sample. This error is of the same order of magnitude as the +0.0004 pH units offset estimated for the SAMI-pH system [26]. The deviation from the

Fig. 5. Map of surface water pH_{tot} in European shelf waters determined during research cruise D366.

absorbance ratio as a function of indicator concentration. The error due to the Schlieren effect has been estimated to be 0.004 pH units during the cruise D366. This artefact has since been significantly reduced by injecting a volume of indicator in the cell large enough (12 μL here) to obtain the maximum indicator concentration gradients at absorbance values higher than 1.7.

In order to verify the adequacy of the indicator pH correction method, DIC and TA certified reference material (batch 117, Scripps Institution of Oceanography, USA) was analyzed at $25.03 \pm 0.01\,^{\circ}C$ later on with the new analytical configuration (*i.e.* with 12 μL of indicator per sample instead of the 5 μL injected per sample during the cruise deployment) to minimize the Schlieren effect and a new solution of indicator prepared from the same thymol blue batch. The discrepancy between measured pH and pH values calculated from DIC and TA values was 0.0011 ± 0.0011 ($n = 20$). The method applied to correct for the indicator perturbation was therefore considered adequate. Finally, the thermistors were calibrated with an accuracy of $0.03\,^{\circ}C$ resulting in a potential error in pH of 0.0004 pH units.

4.7. Cruise data

The automated pH system was operated continuously on the underway seawater supply for a month during the cruise D366 and more than 5000 pH data were obtained. Less than 30 mL of indicator was consumed over the duration of the cruise. Measurements were only interrupted for system performance checks and maintenance. Surface ocean pH data obtained during cruise D366 are presented in Fig. 5. Dissolved inorganic carbon data were used to calculate pH data at *in situ* temperature [48]. The magnitude of the correction was about 0.002 ± 0.001 pH units, whereas measurements at 25 °C would have required a correction of *ca.* 0.2 pH units. The determination of pH at temperatures close to the *in situ* values therefore significantly reduces the potential error introduced by the required temperature corrections. With our system, *in situ* pH can also be obtained using the linear regression proposed by Millero ($dpH/dT = -1.582E{-}2$) [49] which avoids the requirement of a second carbonate parameter.

The observed pH_{tot} along the transect ranged between 7.995 and 8.210, with highest values in the northern North Sea whilst sailing through waters with enhanced biomass, which resulted in CO_2 uptake by marine phytoplankton with a consequent increase in pH. Lowest pH values were observed in the central North Sea in a well-mixed water column which featured enhanced dissolved

organic carbon concentrations (up to 90 μM compared with 65 μM in northern North Sea) and associated enhanced organic matter respiration with a consequent decrease in pH.

5. Conclusion

We report a key step towards the miniaturization of the colorimetric pH sensor with the successful implementation of a simple microfluidic design with a low reagent consumption. Less than 30 mL of indicator was consumed during a month of deployment at sea of the novel pH instrument. This is a great advantage for long term deployment on ships (*e.g.* on FerryBox systems [50]) or moorings. The system demonstrated to be particularly adapted to shipboard deployment with high quality data obtained during a research cruise in European shelf waters. The system featured a short term precision of 0.001 pH unit ($n = 20$) and an accuracy within the range of a certified Tris buffer (0.004 pH units). The optical set up was robust and relatively small with the use of an USB mini-spectrometer, a custom made polymeric flow cell and the LED light source. The simple design of this microfluidic platform proved to be very efficient as it enabled effective mixing of the indicator with the sample, and allowed pH measurements and correction of the indicator effect on the sample pH with a single addition of indicator. The single packaged three wavelengths LED showed the advantages of LEDs light sources (cheap, small, stable with relatively narrow spectrum) but with the additional advantage that it did not require coupling of the light from three separate LEDs. The integration of the signal over the whole of each LED peak reduced signal noise, and indicated the possibility to replace the current spectrophotometer with a small chip mountable mini-spectrophotometer featuring a lower wavelength resolution or with a photodiode. The pH measurement close to *in situ* temperature (+0.2 °C) in the sampling chamber greatly reduced the source of error due to the correction to *in situ* conditions.

References

[1] P.S. Dittrich, K. Tachikawa, A. Manz, Anal. Chem. 78 (2006) 3887–3908.
[2] R.D. Prien, Mar. Chem. 107 (2007) 422–432.
[3] Intergovernmental Panel on Climate Change, CW TeamR.K. Pachauri, A.E. Reisinger, IPPC Climate Change 2007: Synthesis Report, in: Contribution of Working Groups I, II and III to the Fourth Assessment Report of the Intergovernmental Panel on Climate Change, IPCC, Geneva, Switzerland, 2007.
[4] J.G. Canadell, C. Le Quéré, M.R. Raupach, C.B. Field, E.T. Buitenhuis, P. Ciais, T.J. Conway, N.P. Gillett, R. Houghton, G. Marland, Proc. Natl. Acad. Sci. 104 (2007) 18866–18870.
[5] S.C. Doney, Science 328 (2010) 1512.
[6] C.L. Sabine, R.A. Feely, N. Gruber, R.M. Key, K. Lee, J.L. Bullister, R. Wanninkhof, C.S. Wong, D.W.R. Wallace, B. Tilbrook, Science 305 (2004) 367–371.
[7] K. Caldeira, M.E. Wickett, J. Geophys. Res. 110 (2005) 1–12.
[8] M. González-Dávila, Biogeosciences 7 (2010) 1995–2032.
[9] J.E. Dore, R. Lukas, D.W. Sadler, M.J. Church, D.M. Karl, Proc. Natl. Acad. Sci. 106 (2009) 12235.
[10] R.H. Byrne, S. Mecking, R.A. Feely, X. Liu, Geophys. Res. Lett. 37 (2010) L02601.
[11] S.C. Doney, B. Tilbrook, S. Roy, N. Metzl, C. Le Quéré, M. Hood, R.A. Feely, D. Bakker, Deep Sea Res. II: Top. Stud. Oceanogr. 56 (2009) 504–511.

[12] K.S. Johnson, W.M. Berelson, E.S. Boss, Z. Chase, H. Claustre, S.R. Emerson, N. Gruber, A. Kortzinger, M.J. Perry, S.C. Riser, Oceanography (2009) 216–225.
[13] V.M.C. Rérolle, C.F.A. Floquet, M.C. Mowlem, D.P. Connelly, E.P. Achterberg, R.R.G.J. Bellerby, Trend Anal. Chem. 40 (2012) 146–157.
[14] R.G.J. Bellerby, D.R. Turner, G.E. Millward, P.J. Worsfold, Anal. Chim. Acta 309 (1995) 259–270.
[15] R.G.J. Bellerby, A. Olsen, T. Johannessen, P. Croot, Talanta 56 (2002) 61–69.
[16] T.A. DelValls, Cien. Mar. 25 (1999) 345–365.
[17] L.M. Mosley, S.L.G. Husheer, K.A. Hunter, Mar. Chem. 91 (2004) 175–186.
[18] S.M. Ohline, M.R. Reid, S.L.G. Husheer, K.I. Currie, K.A. Hunter, Mar. Chem. 107 (2007) 143–155.
[19] M. Tapp, K. Hunter, K. Currie, B. Mackaskill, Mar. Chem. 72 (2000) 193–202.
[20] Z.A. Wang, X. Liu, R.H. Byrne, R. Wanninkhof, R.E. Bernstein, E.A. Kaltenbacher, J. Patten, Anal. Chim. Acta 596 (2007) 23–36.
[21] S. Aßmann, C. Frank, A. Kötzinger, Ocean Sci. Discuss. 8 (2011) 1339–1367.
[22] E. Kaltenbacher, E. Steimle, R. Byrne, IEEE (2000) 41–45.
[23] X. Liu, Z.A. Wang, R.H. Byrne, E.A. Kaltenbacher, R.E. Bernstein, Environ. Sci. Technol. 40 (2006) 5036–5044.
[24] T.R. Martz, J.J. Carr, C.R. French, M.D. DeGrandpre, Anal. Chem. 75 (2003) 1844–1850.
[25] Y. Nakano, H. Kimoto, S. Watanabe, K. Harada, Y.W. Watanabe, J. Oceanogr. 62 (2006) 71–81.
[26] M.P. Seidel, M.D. DeGrandpre, A.G. Dickson, Mar. Chem. 109 (2008) 18–28.
[27] G. Robert-Baldo, M. Morris, R. Byrne, Anal. Chem. 57 (1985) 2564–2567.
[28] M.D. Gabriel, J.M. Forja, J.A. Rubio, A. Gomez-Parra, Cien. Mar. 31 (2005) 309–318.
[29] I. Ogilvie, V. Sieben, C. Floquet, R. Zmijan, M. Mowlem, H. Morgan, J. Micromech. Microeng. 20 (2010) 065016.
[30] C.F.A. Floquet, V.J. Sieben, A. Milani, E.P. Joly, I.R.G. Ogilvie, H. Morgan, M.C. Mowlem, Talanta (2011) 235–239.
[31] A.D. Beaton, V.J. Sieben, C.F.A. Floquet, E.M. Waugh, S.A.K. Bey, I.R.G. Ogilvie, M.C. Mowlem, H. Morgan, Sens. Actuators B: Chem. (2011) 1009–1014.
[32] V.J. Sieben, C.F.A. Floquet, I.R.G. Ogilvie, M.C. Mowlem, H. Morgan, Anal. Methods 2 (2010) 484–491.
[33] H. Zhang, R.H. Byrne, Mar. Chem. 52 (1996) 17–25.
[34] X. Liu, M.C. Patsavas, R.H. Byrne, Environ. Sci. Technol. (2011) 4862–4868.
[35] W. Yao, X. Liu, R.H. Byrne, Mar. Chem. 107 (2007) 167–172.
[36] T. Clayton, R. Byrne, Deep Sea Res. I: Oceanogr. Res. Pap. 40 (1993) 2115–2129.
[37] K. Friis, A. Körtzinger, D.W.R. Wallace, Limnol. Oceanogr. Methods 2 (2004) 126–136.
[38] M. Chierici, A. Fransson, L.G. Anderson, Mar. Chem. 65 (1999) 281–290.
[39] G. Taylor, Proc. Roy. Soc. Lond. A: Math. Phys. Sci. 219 (1953) 186–203.
[40] D.A. Edwards, H. Brenner, Macrotransport Processes, Butterworth–Heinemann, 1993.
[41] G.C.Y. Chan, W.T. Chan, J. Chem. Educ. 78 (2001) 1285–1288.
[42] P.C. Hauser, T.W.T. Rupasinghe, N.E. Cates, Talanta 42 (1995) 605–612.
[43] I. Ogilvie, V. Sieben, M. Mowlem, H. Morgan, Anal. Chem. (2011) 4814–4821.
[44] D. Pierrot, E. Lewis, D.W.R. Wallace, MS Excel Program Developed for CO$_2$ System Calculations. ORNL/CDIAC-105a. Carbon Dioxide Information Analysis Center, Oak Ridge National Laboratory, U.S. Department of Energy, Oak Ridge, Tennessee, 2006, http://dx.doi.org/10.3334/CDIAC/otg.CO2SYS_XLS_CDIAC105a
[45] C. Mehrbach, C.H. Culberson, J.E. Hawley, R.M. Pytkowicz, Limnol. Oceanogr. (1973) 897–907.
[46] A. Dickson, F. Millero, Deep Sea Res. I: Oceanogr. Res. Pap. 34 (1987) 1733–1743.
[47] A.G. Dickson, J. Chem. Thermodyn. 22 (1990) 113–127.
[48] K.A. Hunter, Deep Sea Res. I: Oceanogr. Res. Pap. 45 (1998) 1919–1930.
[49] F.J. Millero, Chem. Rev. 107 (2007) 308–341.
[50] D. Hydes, F. Colijn, W. Petersen, F.S.D.K. Mills, D. Durand, B.N. Niva, in: J. Hall, D.E. Harrison, D. Stammer (Eds.), Proceedings of OceanObs'09, 2010, ESA Publication WPP-306.